ELSEVIER

Journal of Hydrology 204 (1998) 168–181

Journal of Hydrology

Chaotic characteristics of the Southern Oscillation Index time series

Akira Kawamura[a,*], Alistair I. McKerchar[b], Robert H. Spigel[c], Kenji Jinno[a]

[a]*Department of Civil Engineering, Kyushu University, Fukuoka 812, Japan*
[b]*National Institute of Water and Atmospheric Research Ltd (NIWA), P.O. Box 8602, Christchurch, New Zealand*
[c]*Department of Civil Engineering, University of Canterbury, Christchurch, New Zealand*

Received 26 March 1997; revised 26 September 1997; accepted 26 September 1997

Abstract

The monthly time series of the Southern Oscillation Index (SOI) is analysed to examine its chaotic characteristics. Three schemes, moving average, low-pass filter and nonlinear smoothing, were used to reduce noise and enhance chaotic properties. Autocorrelation and spectral characteristics, as well as three chaos-oriented properties — phase space trajectory, the largest Lyapunov exponent and correlation dimension — were then examined.

No significant signs of chaotic behaviour were found for either the noise-reduced SOI time series or the raw one. Although it contains long-term periodicity, the SOI time series is considered to be stochastic rather than chaotic from the viewpoint of dynamical systems theory. © 1998 Elsevier Science B.V.

Keywords: Southern Oscillation Index; Chaos; Nonlinear smoothing; Lyapunov exponents; Correlation dimension; Mean sea-level pressure

1. Introduction

The Southern Oscillation is a phenomenon which affects large-scale atmospheric and oceanographic features of the tropical Pacific Ocean. The oscillation can be characterized by indices based on variations in either sea-surface temperatures or differences in barometric pressures. Its best-known extremes are El Niño events. Analyses of the Southern Oscillation Index (SOI) and its relationships with hydrological phenomena have been presented by many researchers in recent decades (e.g., Trenberth, 1984; Gordon, 1986; Opoku-Ankomah and Cordery, 1993; Moss et al., 1994; Mullan, 1995; Piechota and Dracup, 1996; McKerchar et al., 1996; Stone et al., 1996). Many El Niño Southern Oscillation (ENSO) models incorporating ocean–atmosphere dynamics (e.g., Zebiak and Cane, 1987; Jin et al., 1994; Tziperman et al., 1994) have also been proposed.

Recent studies that consider the chaotic behaviour of time series, such as sunspots, have indicated that better predictions can be made by using developments in dynamical systems theory (Mundt et al., 1991; Jinno et al., 1995). Chaotic dynamics arise in nonlinear deterministic systems that are very sensitive to initial conditions (so-called "butterfly effect") and yield outputs that are indistinguishable by standard statistical techniques from a stochastic process (Rodriguez-Iturbe et al., 1989). A chaotic time series originates from a nonlinear system with a small number of degrees of freedom, whereas a stochastic time series arises from a system with many degrees of freedom (Jeong and Rao, 1996). There is now considerable interest in identifying chaos in natural or

* Corresponding author.

PII S0022-1694(97)00129-7

experimentally observed time series. Hense (1987) has estimated correlation dimension of three 84 year Southern-Oscillation-related monthly time series: the precipitation at Nauru, the sea-surface temperature (SST) at Puerto Chicama and the surface pressure at Darwin. He hypothesized the existence of a strange attractor for the precipitation and SST time series with a correlation dimension between 2.5 and 6.0. Some ENSO models can also generate chaotic behaviour (Jin et al., 1994; Tziperman et al., 1994). The SOI time series itself, however, which is commonly defined as the standardized sea-level barometric pressure difference between Tahiti and Darwin, has not yet been checked in detail for chaotic characteristics; this is especially true for the noise-reduced SOI time series.

The main purpose of this paper is to find out whether the SOI time series is chaotic or not. We try to identify the essential features of the SOI when viewed as a dynamic system. Several data analysis techniques need to be combined to ascertain chaotic behaviour. In this study, three schemes are used to reduce noise in the time series and enhance its chaotic features. Then, three methods for detecting and identifying the chaotic characteristics of a time series, i.e., drawing its phase space trajectory, checking Lyapunov exponents and evaluating correlation dimension, are applied to the noise-reduced series as well as the raw data, after autocorrelation and spectral characteristics have been examined. If a time series can be identified as deterministic chaos, then the knowledge of its underlying characteristics would make short-term predictions possible (in this case of the SOI) by setting the system on a fractal trajectory (strange attractor), although chaotic systems are unpredictable in the long term (e.g., Casdagli, 1989; Sugihara and May, 1990; Jinno et al., 1995; Berndtsson et al., 1994; Kawamura et al., 1994a, b).

2. Data

Several indices have been used to monitor the Southern Oscillation. One commonly used SOI is derived from values of the monthly mean sea-level pressure difference between Papeete, Tahiti

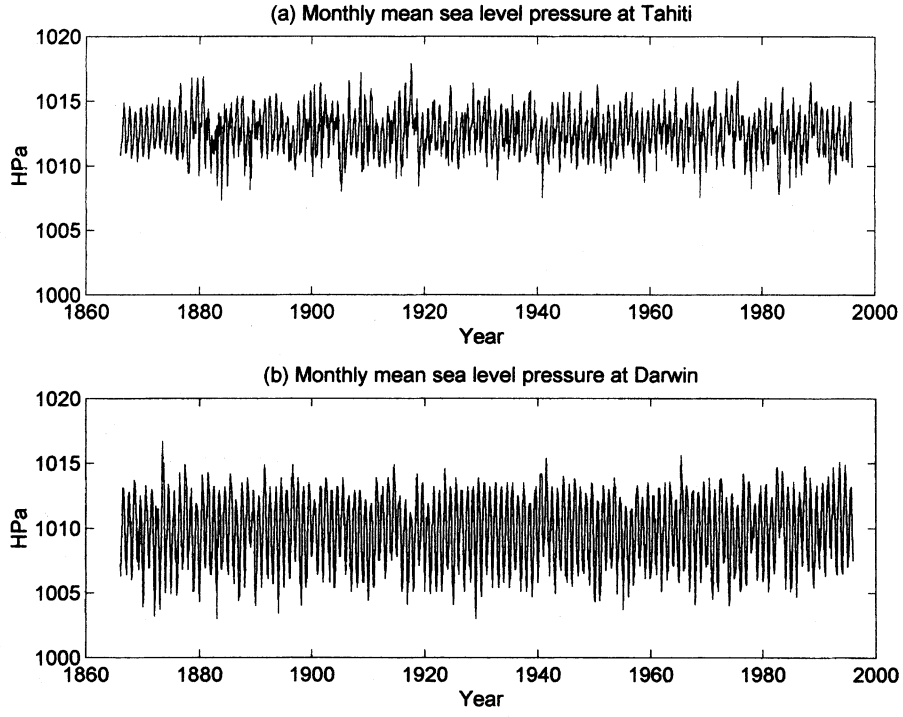

Fig. 1. Monthly mean sea-level pressure time series at (a) Tahiti and (b) Darwin.

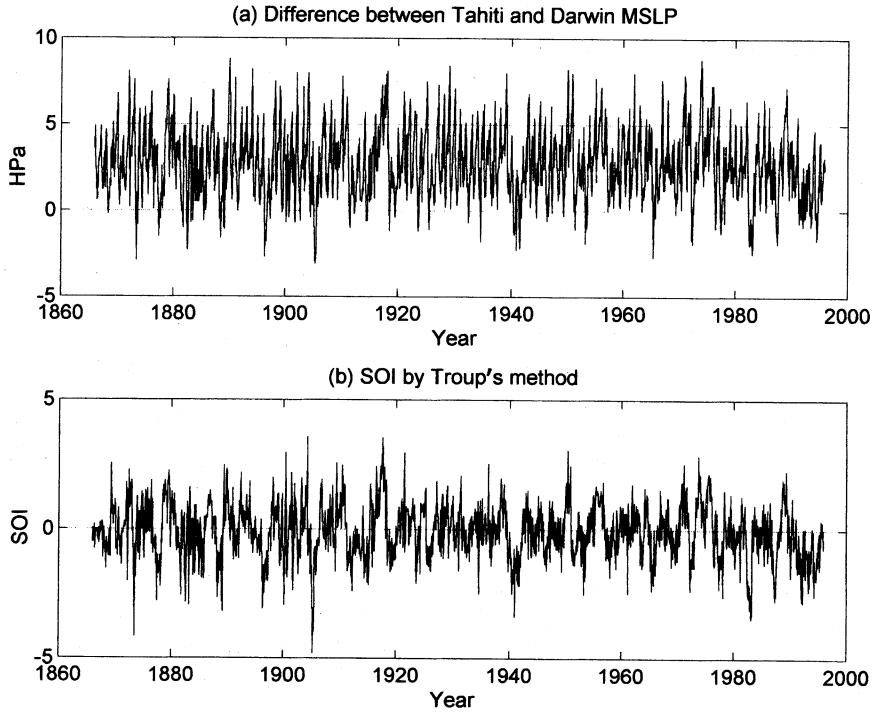

Fig. 2. (a) Monthly mean sea-level pressure difference between Tahiti and Darwin; (b) SOI time series by Troup's method.

(149.6°W, 17.5°S) and Darwin, Australia (130.9°E, 12.4°S). The data used in this study for calculation of SOI are 130 year monthly mean sea-level pressure data at Tahiti and Darwin from January 1866 to December 1995. All mean sea-level pressure data were obtained from Ropelewski and Jones (1987) and Allan et al. (1991), who carefully infilled all the missing data by correlation with data from other observation stations. Because of missing data, some years before about 1920 are somewhat less reliable than the later values. However, in order to determine the chaotic characteristics from a time series, a long continuous series is essential. Fig. 1 shows monthly mean sea-level pressure time series at Tahiti and Darwin from 1866 to 1995. Both series have an obvious one year cycle, and the mean sea-level pressure at Tahiti is usually higher than that at Darwin.

Two commonly used methods to compute the SOI from mean sea-level pressure at Tahiti and Darwin are Troup's method and the Climate Prediction Centre's method. Troup's method (Troup, 1965; McBride and Nicholls, 1983) first takes the difference between pressures at Tahiti and Darwin (Fig. 2(a)). Then the difference series is normalized to mean zero and a standard deviation of one by subtracting the monthly mean values and dividing by the monthly standard deviations, usually using the period from 1951 to 1980 as the base period for the computation of the mean and standard deviation. This normalized time series is defined as Troup's SOI (Fig. 2(b)). Note that a standard deviation of 10 is also commonly used. The Climate Prediction Centre's method (Ropelewski and Jones, 1987), on the other hand, first normalizes each monthly pressure value, and then takes the differences. The time series of difference is then normalized again, giving a series known as the Climate Prediction Centre's SOI. Fig. 3 shows the difference between the two SOI series. As seen in Fig. 3 and as pointed out by McBride and Nicholls (1983) and Ropelewski and Jones (1987), the difference is very small. Therefore, in the following study, only the results for the Troup's SOI time series are shown. Analyses have shown that the chaotic characteristics of the Climate Prediction Centre's SOI time series are the same as those of Troup's SOI time series.

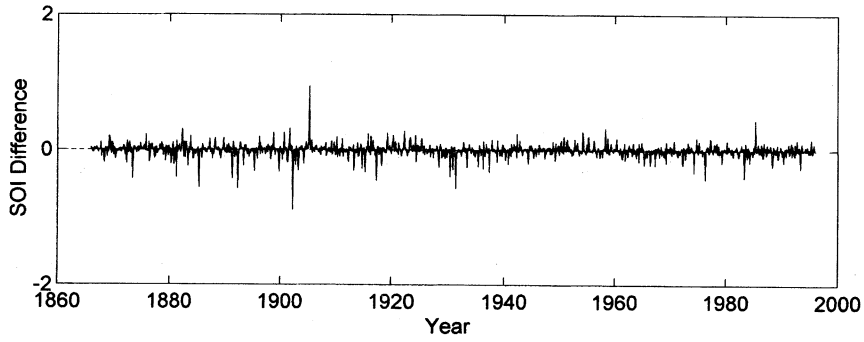

Fig. 3. Difference between Troup's SOI and the Climate Prediction Centre's SOI.

3. Noise reduction schemes

Observed hydrometeorological time series generally contain noise. Methods for identifying chaotic characteristics are very sensitive to noise. Therefore, time series need firstly to be cleaned by a noise reduction scheme (Grassberger et al., 1991). Berndtsson et al. (1994) indicate that raw time series of sunspots, temperature and precipitation variables do not show any chaotic deterministic properties, but after noise reduction, all three variables display a low-dimensional chaotic behaviour. In the present study, two linear and one nonlinear noise reduction schemes were applied to the SOI time series: moving average, low-pass filter and nonlinear smoothing.

Moving average and low-pass filter are commonly used for noise reduction of any type of time series. These schemes are especially designed to reduce high-frequency components of the time series, which are usually regarded as noise. It is useful and informative to see how, in practice, these commonly used linear noise reduction schemes affect the following chaos-oriented properties — phase space trajectory, Lyapunov exponents and correlation dimension.

The moving average used here is simply an equally weighted running mean, with a running period of 25 months. As a result, the unsmoothed first and last 12 months in the time series are neglected in the following analysis.

The low-pass filter used in the study is expressed by

$$y(t)=(1-\alpha)x(t)+\alpha y(t-1) \tag{1}$$

where t is the time step; x is the raw SOI data; y is the smoothed SOI data; and α is the smoothing coefficient ($0 \leq \alpha \leq 1$). Here, α is selected as 0.6. The frequency characteristics of this filter have been given by Kawamura et al. (1985).

The nonlinear smoothing algorithm used in this study was proposed by Schreiber (1993). It is a simple nonlinear noise reduction scheme especially developed for dimension estimation. The general idea of the nonlinear smoothing is to replace each coordinate in the time series $\{x_i\}$, $i=1,\ldots,T$, by an average value over a suitable neighbourhood in the phase space. The neighbourhoods are defined in a phase space reconstructed by delay coordinates. To define the neighbourhoods, first fix the positive integers k and l, and construct embedding vectors $\mathbf{x}_i$:

$$\mathbf{x}_i=[x_{i-k},\ldots,x_{i+l}] \tag{2}$$

A radius η is chosen for the neighbourhoods. For each coordinate in $\mathbf{x}_i$ find the set Ω_i^η of all neighbours $\mathbf{x}_j$ for which

$$\sup\{|x_{j-k}-x_{i-k}|,\ldots,|x_{j+l}-x_{i+l}|\} \equiv \|\mathbf{x}_j-\mathbf{x}_i\|_{\sup}<\eta \tag{3}$$

where the symbol "sup" denotes supreme, or the highest value of the elements. Consequently, the present coordinate x_i is replaced by its mean value in Ω_i^η:

$$x_i^{coor}=\frac{1}{|\Omega_i^\eta|}\sum_{\Omega_i^\eta}x_j \tag{4}$$

Here, k and l in Eq. (3) are both selected as 12 months. As a result, the first and last 12 months of the SOI time series are not smoothed, and those

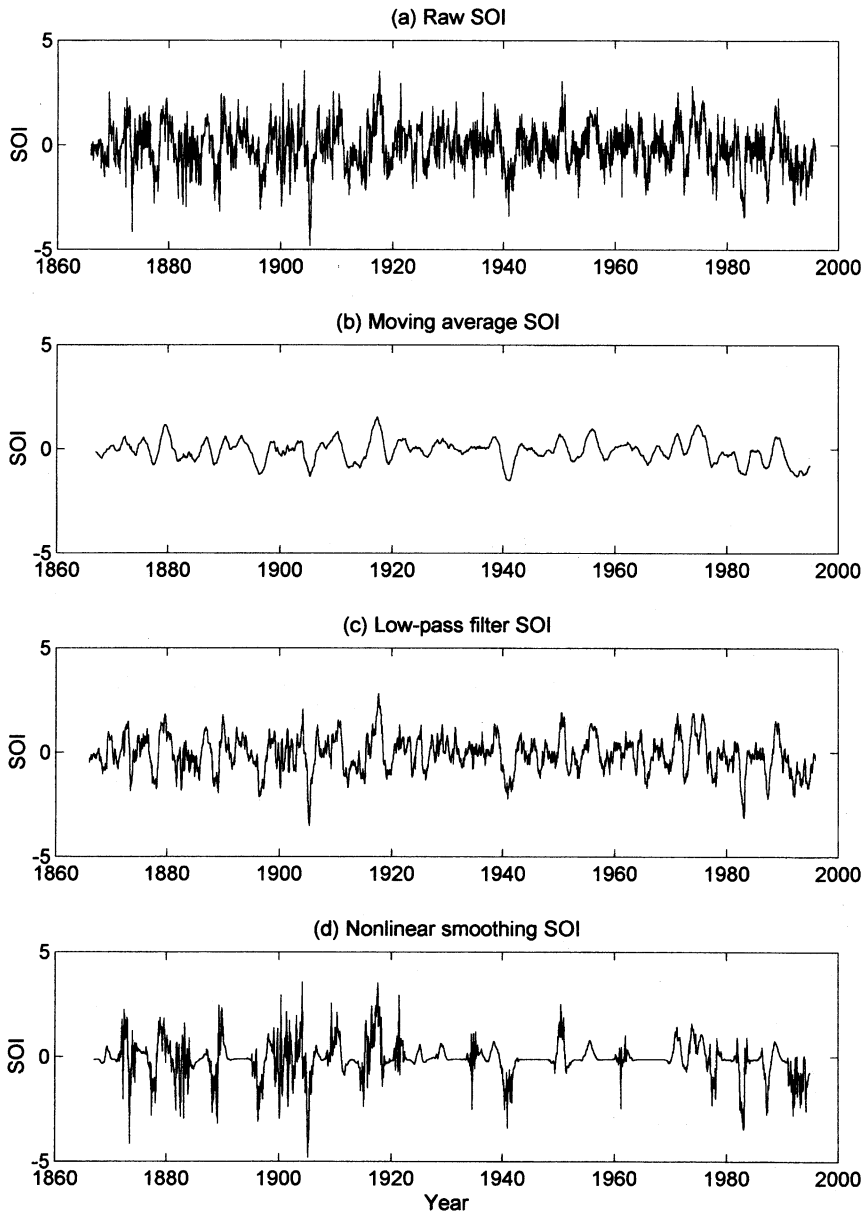

Fig. 4. Time series of (a) raw SOI data and noise-reduced data by (b) moving average, (c) low-pass filter and (d) nonlinear smoothing.

unsmoothed periods are neglected in the following analysis.

Fig. 4 shows the raw SOI time series and three noise-reduced time series obtained by using the above-mentioned schemes. The nonlinear smoothing time series was obtained after four iterations in the noise reduction algorithm (Eqs. (3) and (4)).

4. Autocorrelation and spectral analysis

Various definitions have been proposed for deterministic chaos. According to Ott (1981): (1) it is aperiodic, (2) its autocorrelation function converges to zero with the increase of lag time, and (3) it is extremely sensitive to initial conditions.

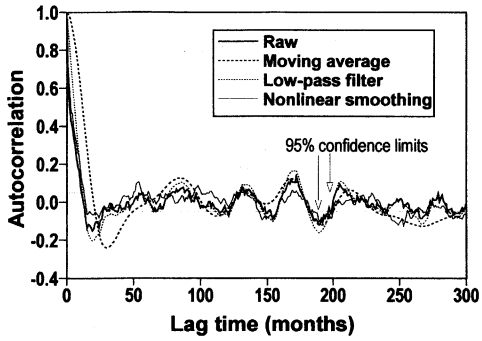

Fig. 5. Autocorrelation functions for SOI time series.

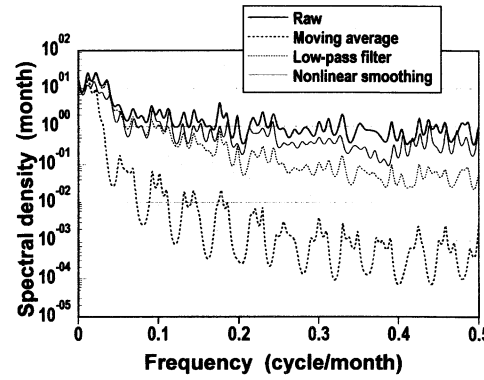

Fig. 6. Power spectra for SOI time series.

Here, we check the autocorrelation and spectral characteristics of the raw and noise-reduced SOI time series before special chaos-oriented methods are applied in the following section.

Fig. 5 shows the autocorrelation functions for four (raw, moving average, low-pass filter and nonlinear smoothing) SOI time series. From the figure, the autocorrelation functions for the moving average and low-pass filter time series show long smoothed periodicity and do not converge to zero with increasing lag time. The raw SOI time series has small fluctuations as well as the longer ones, and does not seem to converge to zero, either. The nonlinear smoothing series is closer to zero than any of the other time series, but it is difficult to say whether it converges to zero or not.

The lag time at which the autocorrelation function attains the value of zero for the first time is 12 months for raw, low-pass filter and nonlinear smoothing time series; this observation is necessary for the choice of delay time in the next section.

Fig. 6 shows the results of spectral analysis for the above-mentioned four SOI time series. Spectral analysis is carried out to check on periodicity and to see if the time series has the broadband spectra necessary for chaos. Here we used Burg's Maximum Entropy Method (MEM) (Nobes et al., 1991) because it has a higher frequency-resolution ability than Fast Fourier Transform. The spectral density of the raw SOI series exhibits prominent long period components of about 7 and 4 years, indicated as the first two peaks in the spectral density line at frequencies of 0.012 and 0.022 cycle month^{-1}. The third peak at 0.035 cycle month^{-1} corresponds to a component with a period of 28 month. Shorter-period components less than 2 years are an order of magnitude smaller than the longer-period components, but the spectrum still exhibits a broadband character. The raw SOI time series could be described as periodic with white noise, because white noise also has a broadband spectrum with constant spectral density for all frequency components.

The spectrum for the low-pass-filtered series shows significant energy in the low-frequency components with periods greater than 2 years, in common with the raw SOI spectrum, but high-frequency components are greatly reduced by the filtering. The moving average method reduces the energy content of high frequencies still further, with significant energy remaining only in the 7 year component (Fig. 6). Nonlinear smoothing, on the other hand, reduces the whole range of frequencies by almost the same amount, while maintaining a broadband spectrum.

It is clear that spectral analysis is not very helpful in distinguishing chaos from white noise, because both have broadband spectra. In the following sections, three chaos-oriented properties are examined to detect and identify the chaotic characteristics of SOI time series. The properties are phase space trajectory, Lyapunov exponents and correlation dimension.

5. Phase space trajectory

Dissipative dynamical systems which exhibit chaotic behaviour often have a strange attractor in phase space (Grassberger and Procaccia, 1983). We first reconstruct the attractor by using the method of

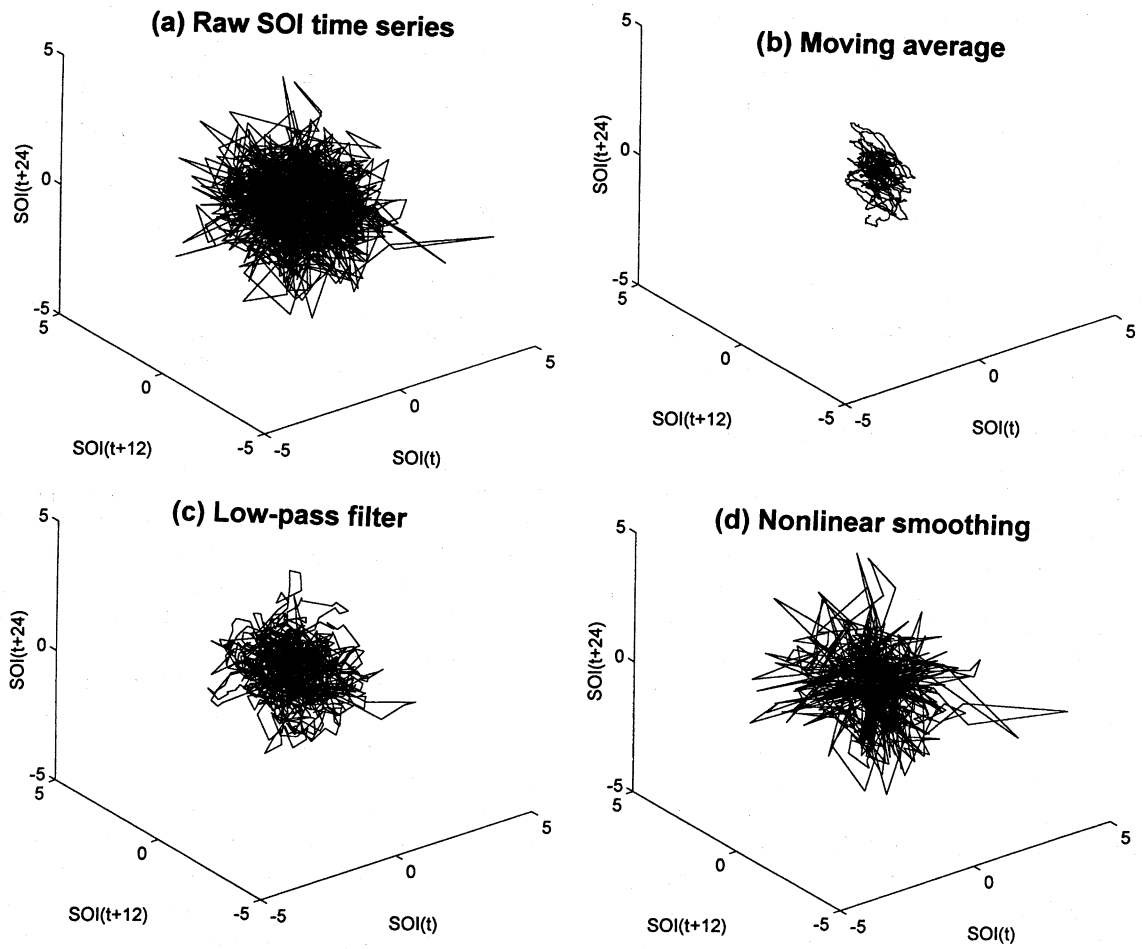

Fig. 7. Three-dimensional phase space trajectory for SOI time series for (a) raw, (b) moving average, (c) low-pass filter and (d) nonlinear smoothing.

time-delay coordinates in order to check for the existence of deterministic dynamics that could produce chaotic behaviour. To check the behaviour, we use the phase space trajectory of the time series, which plots a time series on one axis, versus the same series but with a time delay on the other axes. Presented mathematically, let $\{x(t)\}$ be a discrete sample time series. A state space vector X_t is constructed, or embedded from m consecutive values of the time series into a phase space whose coordinates are described by

$$X_t = [x(t), x(t+\tau), \ldots, x(t+(m-1)\tau)] \quad (5)$$

where τ is the delay time, and the dimension m of the vector is known as the embedding dimension. Following Eq. (5), a new time series of the state space vectors $X_1, X_2, \ldots, X_N$ is generated. Each vector X_t describes a point in an m-dimensional phase space. Thus the sequence of these vectors defines a trajectory.

Fig. 7(a)–Fig. 7(d) show the three-dimensional phase space trajectories for the raw, moving average, low-pass filter and nonlinear smoothing SOI time series, respectively. In these figures, the generated time series of the state space vectors are connected with straight lines to indicate clearly their time evolution, even though the transition values between one space vector and the next are not known.

In the above case, the delay time or lag time τ must be chosen so as to result in points that are not

correlated to previously plotted points. Thus, a first choice of τ should be in terms of the decorrelation time of the time series (Tsonis et al., 1993). A straightforward procedure is to consider the decorrelation time equal to the lag at which the autocorrelation function for the first time attains the value of zero. By using this consideration, τ was chosen as 12 months (Fig. 5). This lag value was also used for the following calculations of Lyapunov exponents and correlation dimension.

If a time series has chaotic properties, the state space vector X_t will be attracted to the particular region of the phase space known as the strange attractor, as is seen in nonlinearly smoothed sunspot time series (Jinno et al., 1995) or nonlinearly smoothed temperature time series (Berndtsson et al. 1994); raw time series of those variables do not show any chaotic deterministic properties.

We cannot see any attractors in the phase space trajectory for the raw SOI time series (Fig. 7(a)). The phase space trajectory for the moving average series is much smaller than the raw one (Fig. 7(b)). Attractors are not readily apparent in Fig. 7(b), but it is a little more difficult to judge than for the raw data. The trajectory for low-pass filter series is also smaller than for the raw one, but no attractors are evident (Fig. 7(c)). For nonlinear smoothing trajectory, the randomness itself looks reduced compared with that of the raw data, but the overall trajectory maintains the same size and shape as that of the raw data (Fig. 7(d)). However, the nonlinearly smoothed data do not show any clear attractors, in contrast to those found in above-mentioned nonlinearly smoothed sunspot or temperature time series.

Note that Fig. 7(a)–Fig. 7(d) show projections of phase space trajectories onto three-dimensional space, so that the fact that no attractors can be seen does not imply that they do not exist when embedding in higher-dimensional space. However, a strange attractor of higher-dimensional space often reflects its shape onto the lower-dimensional space as well. For instance, the trajectory onto the two-dimensional phase space (embedding dimension $m = 2$ in Eq. (5)) reconstructed from the time series of variable x of the Lorenz equations (Lorenz, 1963; Kawamura et al., 1994a; Kawamura et al., 1994b), a well-known set of chaotic differential equations with three variables, shows a clear strange attractor.

6. Lyapunov exponents

The limits of predictability are set by how fast the trajectories diverge from nearby initial conditions. The speed of divergence is measured by the so-called Lyapunov exponents (Rodriguez-Iturbe et al., 1989). Lyapunov exponents are the average exponential rates of divergence or convergence of nearby orbits in phase space. Any system containing at least one positive Lyapunov exponent is defined to be chaotic, with the magnitude of the exponent reflecting the time scale at which system dynamics become unpredictable (Wolf et al., 1985).

To define the Lyapunov exponents, imagine an infinitesimal hypersphere of initial conditions in n-dimensional phase space. There is one Lyapunov exponent for each degree of freedom of the system. We observe the evolution of the hypersphere as time progresses. The hypersphere will be deformed into a hyper-ellipsoid because of the evolution of the system. Then the ith Lyapunov exponent can be defined in terms of the length of the ith principal axis, p_i, of the ellipsoid by

$$\lambda_i = \lim_{t \to \infty} \frac{1}{t} \ln \frac{p_i(t)}{p_i(0)} \tag{6}$$

where the λ_is are ordered from largest to smallest in an algebraic sense (Mundt et al., 1991; Wolf et al., 1985). A minimum condition for chaos is that the largest Lyapunov exponent, λ_1, be positive.

Wolf et al. (1985) developed a method of determining λ_1 from a time series by using a relatively simple procedure. This algorithm is robust over a large range of input parameters and relatively accurate for small, noisy data sets (Mundt et al., 1991). We used this algorithm to obtain the largest Lyapunov exponent. The delay time τ was chosen as 12 months, as mentioned earlier. We varied the embedding dimension m from 3 to 9. The algorithm also requires specification of a parameter called EVOLV which controls the length of time that a given trajectory is allowed to evolve before each successive estimate of the largest Lyapunov exponent is made. Our calculations were carried out for varied values of parameter EVOLV of 10, 15, 20, 25 and 30.

A typical implementation of the algorithm for

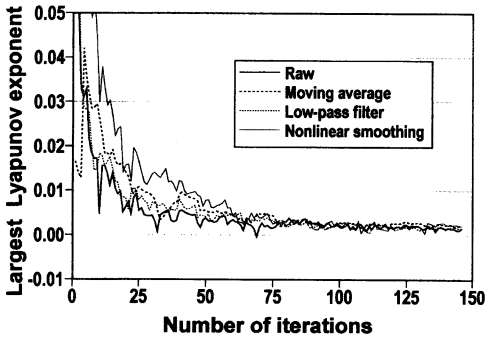

Fig. 8. The largest Lyapunov exponent estimation for delay time τ = 12, embedding dimension m = 6 and parameter EVOLV = 10.

the four SOI time series is shown in Fig. 8 for τ = 12 months, m = 6 and EVOLV = 10. Note the convergence of the estimate of the largest Lyapunov exponent as the number of iterations increase; all four largest Lyapunov exponents converge to almost the same value of around 0.002 month^{-1}. We obtained a reasonable variation of the convergence values of the largest Lyapunov exponents from roughly 0.001 to 0.01 month^{-1} according to the change of embedding dimension m and the parameter EVOLV, but in all cases the estimated convergence largest Lyapunov exponent was positive. As mentioned above, positive largest Lyapunov exponent indicates chaotic dynamics, but the value itself is quite close to zero and should only be interpreted as an order of magnitude. Although this algorithm gives a good estimation of the largest Lyapunov exponent for noise-free synthetically generated time series from chaotic dynamics, the estimation for experimental time series is still relatively imprecise (Rodriguez-Iturbe et al., 1989). In addition, computations implemented by us using this algorithm have shown that if the estimation is carried out for the synthetically generated normally distributed white noise time series whose length is the same as SOI time series, it also yields positive largest Lyapunov exponents of about 0.002–0.005 month^{-1}. This kind of behaviour is also reported by Rodriguez-Iturbe et al. (1989). Therefore, the positive largest Lyapunov exponents obtained for the SOI time series can also be interpreted as having been derived from a stochastic time series with many degrees of freedom (Jeong and Rao, 1996).

7. Correlation dimension

Strange attractors are typically characterized by a fractal dimension d which is smaller than the number of degrees of freedom F, $d < F$ (Grassberger and Procaccia, 1983). There are several ways to define the fractal dimension. In this paper we use the correlation dimension introduced by Grassberger and Procaccia (1983), estimated according to the algorithm given by Grassberger (1990). This algorithm is now the most popular and is commonly used for fractal dimension estimation, although some shortcomings have been pointed out and some improved methods have been proposed recently (e.g., Scargle, 1990; Judd, 1992).

We now describe briefly the Grassberger and Procaccia algorithm. As mentioned before, if the time series is chaotic, sufficiently close trajectories will be attracted to particular regions of the phase space known as strange attractors. The points will thus be partially correlated (Jeong and Rao, 1996). A measure of the spatial correlation is the correlation integral $C(N,r,m)$ which is approximated by

$$C(N,r,m)=\frac{2}{N(N-1)}\sum_{j=1}^{N}\sum_{i=j+1}^{N}\Theta\left(r-|X_i-X_j|\right) \qquad (7)$$

where Θ is the Heaviside function defined by $\Theta(s)$ = 0 for $s < 0$ and $\Theta(s) = 1$ for $s > 0$. In the limit $N \rightarrow \infty$, $C(N,r,m) \rightarrow C(r,m)$ (Ding et al., 1993). The double sum counts the number of pairs (i,j) whose distance $|X_i - X_j|$ is less than r. For small values of r, the correlation integral $C(r,m)$ exhibits a power-law dependence on r:

$$C(r)\sim r^{d} \qquad (8)$$

where d is the correlation dimension of the attractor. The dimension d of the attractor is given by the slope of log $C(r)$ for the slope of log r according to:

$$\log C(r)=d|\log r| \qquad (9)$$

For chaotic data, d will approach a constant value as embedding dimension m is increased. That constant value is an estimate of the correlation dimension which measures the local structure of the strange attractor.

The dimension d of the strange attractor indicates at least how many variables are necessary to describe evolution in time. For example, d = 2.5 indicates

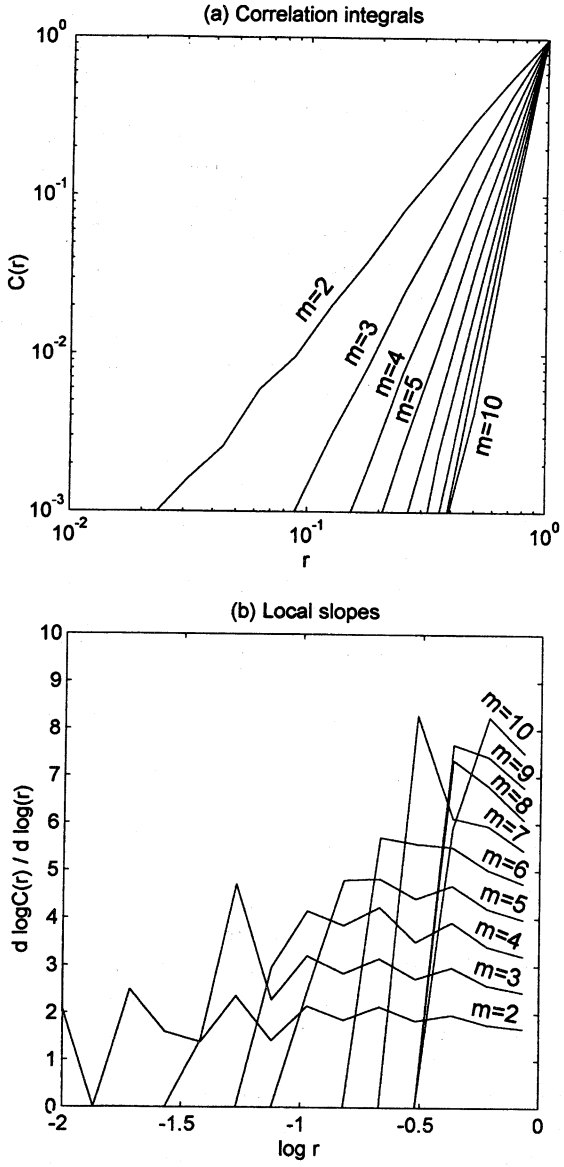

Fig. 9. (a) Correlation integral $C(r)$ versus distance r for various embedding dimension m for raw SOI time series; (b) their local slopes $d \log C(r)/d \log r$.

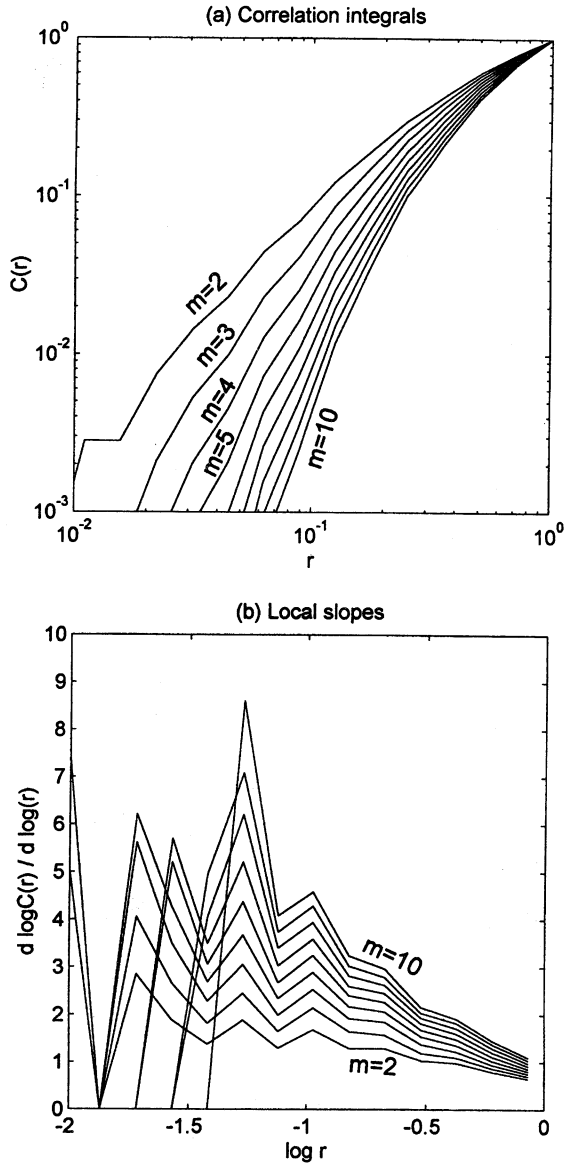

Fig. 10. Same as Fig. 9 but for moving average SOI time series.

that a time series can be described by a system equation containing three independent variables (Berndtsson et al., 1994). Researchers who have investigated chaotic behaviour with this algorithm include Nicolis and Nicolis (1984) and Fraedrich (1986) for climatic records, Rodriguez-Iturbe et al. (1989) for a rainfall record, Mundt et al. (1991) and Jinno et al. (1995) for sunspot series, and Jeong and Rao (1996) for tree ring records.

Fig. 9(a), Fig. 10(a), Fig. 11(a), Fig. 12(a) show the correlation integrals $C(r)$ on logarithmic scales as a function of distance r by varying embedding dimension m from 2 to 10. They are for raw, moving average, low-pass filter and nonlinear smoothing SOI time series, respectively. Fig. 9(b), Fig. 10(b), Fig. 11(b), Fig. 12(b), on the other hand, show

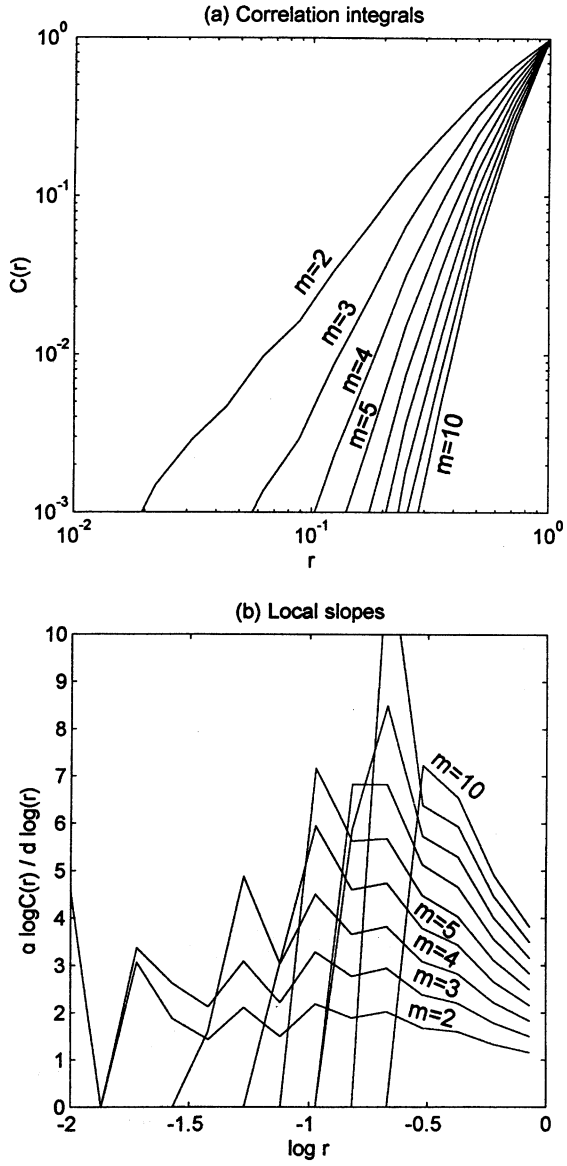

Fig. 11. Same as Fig. 9 but for low-pass filter SOI time series.

the local slopes $\{d \log C(r)/d \log r\}$ for the same data. In these figures, distance r is normalized by its maximum value (the maximum value is taken as one). If the slopes converge to a constant value with increase of embedding dimension m, the convergent slope is regarded as the correlation dimension d of the time series.

From Fig. 9, the slopes for raw SOI time series increase almost in proportion to the increase of m, which is typical of random data (e.g., Fraedrich, 1986; Rodriguez-Iturbe et al., 1989). So we can say that the raw SOI time series is stochastic rather than chaotic. The same can be said for the low-pass filter series (Fig. 11) whose rate of increase in slope is just a little smaller than for the raw data. For the moving average series (Fig. 10), the $C(r)$ lines are curved convex upwards, whereas those for raw SOI time series are almost straight (Fig. 9(a)). This means that the slopes of $C(r)$ lines are decreased with the increase of distance r (Fig. 10(b)). However, the slopes increase as embedding dimension m is increased, although the rate of increase is smaller than that for the raw data. Hence neither low-pass filter nor moving average series show chaotic behaviour characteristic of low-dimensional deterministic chaos. Note that the bigger m becomes, the more data the algorithm requires for accurate calculations of correlation integral, and owing to limits on the number of available data, the algorithm tends to underestimate fractal dimension for the larger m (Tsonis et al., 1993).

The results for the nonlinear smoothing time series (Fig. 12) contrast markedly with those for the other ones. First, the calculated correlation integral $C(r)$ is almost the same for any embedding dimension m. This means the slopes of $\log C(r)$ quickly approach their convergent value with the increase of m. In other words, nonlinear smoothing can sensitively estimate its correlation dimension. Secondly, the convergent slope is less than one, i.e., correlation dimension $d < 1$. One might think from these results that this time series has a simple attractor, but actually it has a random-looking phase space trajectory (Fig. 7(d)). The correlation dimension d is less than one, which would indicate a chaotic series in one dimension because, as mentioned before, d indicates the necessary variables to describe the time series. However, this is forbidden according to Poincare–Bendixson theorem which states that a continuous one- or two-dimensional system cannot exhibit a chaotic behaviour in a bounded region of the phase space (Hense, 1987). Therefore, nonlinearly smoothed SOI time series cannot be considered chaotic, either, even though it has convergent slope in its logarithmic plots of $C(r)$ versus r.

Here, note that smoothing a time series for chaotic dynamics analysis may alter the character of the series

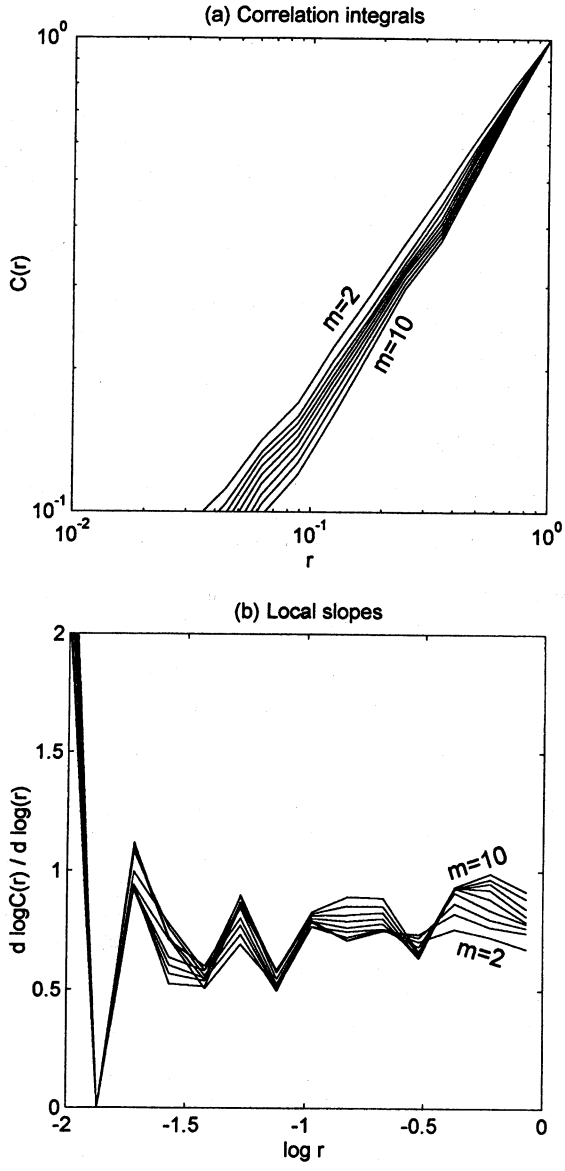

Fig. 12. Same as Fig. 9 but for nonlinear smoothing SOI time series.

and artificially reduce the dimensionality. In other words, it is almost impossible to distinguish between high-dimensional nonlinear dynamics and stochasticity.

8. Conclusions

The results obtained in this study indicate no significant sign of chaotic behaviour in either raw SOI time series or noise-reduced ones using moving average, low-pass filter and nonlinear smoothing methods. Raw, moving average and low-pass filter SOI time series (especially the raw one) were identified as stochastic rather than chaotic, even though they contain long-term periodic components. This may be a numerical artefact arising from the way the SOI time series is derived. The process of normalizing the SOI time series (defined as the difference series of mean sea-level pressures following the subtraction of its annual cycle) results in the noise level becoming dominant compared with the hidden, underlying system dynamics (if any). Furthermore, the properties of two commonly used linear noise reduction schemes for applying these to chaos-oriented methods are studied from a practical viewpoint. From the results, these schemes are probably not appropriate noise reduction schemes for identifying chaos, because of their considerable attenuation of high-frequency components.

On the other hand, although it is not identified as chaos, nonlinearly smoothed SOI time series shows unique features in its correlation dimension estimation; its correlation integrals are insensitive to the value of embedding dimension (namely sensitive estimation of its convergent slope), and its correlation dimension is less than one. This is because nonlinear smoothing method can preserve significant levels of both low- and high-frequency components. However, a correlation dimension less than one precludes chaos.

All of the largest Lyapunov exponents were estimated as positive, which is a necessary condition for chaos, for all four SOI time series considered in this study. However, positive largest Lyapunov exponent would also be estimated for a random time series. Therefore, taking into account the results from other analyses such as phase space trajectory or correlation dimension, the positive largest Lyapunov exponents are considered to derive from the series' stochastic properties.

Acknowledgements

This cooperative research was carried out while the senior author was visiting the National Institute of Water and Atmospheric Research Ltd (NIWA),

Christchurch, New Zealand, in cooperation with the Department of Civil Engineering, University of Canterbury, Christchurch, New Zealand. Financial support was provided by the Japan Society for the Promotion of Science (JSPS). This support is gratefully acknowledged. Provision of valuable data by Dr Phil D. Jones is sincerely appreciated. We also wish to thank Dr Ronny Berndtsson for helpful comments.

References

Allan, R.J., Nicholls, N., Jones, P.D., Butterworth, I.J., 1991. A further extension of the Tahiti–Darwin SOI, early ENSO events and Darwin pressure, J. Climate, 4, 743–749.

Berndtsson, R., Jinno, K., Kawamura, A., Olsson, J., Xu, S., 1994. Dynamical systems theory applied to long-term temperature and precipitation time series, Trends in Hydrol., 1, 292–297.

Casdagli, M., 1989. Nonlinear prediction of chaotic time series, Physica D, 35, 335–356.

Ding, M., Grebogi, C., Ott, E., Sauer, T., Yorke, J.A., 1993. Plateau onset for correlation dimension: when does it occur?, Phys. Rev. Lett., 70 (25), 3872–3875.

Fraedrich, K., 1986. Estimating the dimensions of weather and climate attractors, J. Atmos. Sci., 43 (5), 419–432.

Gordon, N.D., 1986. The Southern Oscillation and New Zealand weather, Mon. Wea. Rev., 114, 371–387.

Grassberger, P., Procaccia, I., 1983. Measuring the strangeness of strange attractors, Physica, 9D, 189–208.

Grassberger, P., 1990. An optimized box-assisted algorithm for fractal dimensions, Phys. Lett. A, 148 (1/2), 63–68.

Grassberger, P., Schreiber, T., Schaffrath, C., 1991. Nonlinear time sequence analysis, Int. J. Bifurc. Chaos, 1, 521–547.

Hense, A., 1987. On the possible existence of a strange attractor for the Southern Oscillation, Beit. Phys. Atmosph., 60 (1), 34–47.

Jeong, G.D., Rao, A.R., 1996. Chaos characteristics of tree ring series, J. Hydrol., 182, 239–257.

Jin, F.-F., Neelin, J.D., Ghil, M., 1994. El Niño on the devil's staircase: annual subharmonic steps to chaos, Science, 264, 70–72.

Jinno, K., Xu, S., Berndtsson, R., Kawamura, A., Matsumoto, M., 1995. Prediction of sunspots using reconstructed chaotic system equations, J. Geophys. Res., 100 (A8), 14774–14781.

Judd, K., 1992. An improved estimator of dimension and some comments on proving confidence intervals, Physica D, 56, 216–228.

Kawamura, A., Ueda, T., Jinno, K., 1985. Analysis of long-term pattern fluctuations in a precipitation sequence (in Japanese with English abstract), J. Jpn. Soc. Civ. Eng., 363 (II-4), 155–164.

Kawamura, A., Matsumoto, M., Jinno, K., Xu, S., 1994. Estimation and prediction for dynamics of chaotic time series (I). On the dependence of Lorenz equation on the initial value and parameters and its prediction by nonlinear least square method (in Japanese with English abstract), Technology Reports of Kyushu University, 67 (5), 513–521.

Kawamura, A., Matsumoto, M., Jinno, K., Xu, S., 1994. Estimation and prediction for dynamics of chaotic time series (II). On the estimation and prediction for dynamics of Lorenz equation by extended Kalman filter (in Japanese with English abstract), Technology Reports of Kyushu University, 67 (5), 523–531.

Lorenz, E.N., 1963. Deterministic nonperiodic flow. J. Atmos. Sci., 20, 130–141.

McBride, J.L., Nicholls, N., 1983. Seasonal relationships between Australian rainfall and the Southern Oscillation, Mon. Wea. Rev., 111, 1998–2004.

McKerchar, A.I., Pearson, C.P., Moss, M.E., 1996. Prediction of summer inflows to lakes in the Southern Alps, New Zealand, using the spring Southern Oscillation Index, J. Hydrol., 184, 175–187.

Moss, M.E., Pearson, C.P., McKerchar, A.I., 1994. The Southern Oscillation index as a predictor of the probability of low streamflows in New Zealand, Water Resour. Res., 30 (10), 2717–2723.

Mullan, A.B., 1995. On the linearity and stability of Southern Oscillation–climate relationships for New Zealand, Int. J. Climatol., 15, 1365–1386.

Mundt, M.D., Maguire, W.B. II, Chase, R.R.P., 1991. Chaos in the sunspot cycle: analysis and prediction, J. Geophys. Res., 96, 1705–1716.

Nicolis, C., Nicolis, G., 1984. Is there a climatic attractor?, Nature, 311 (11), 529–532.

Nobes, D.C., Bloomer, S.F., Mienert, J., Westall, F., 1991. Milankovitch cycles and nonlinear response in the quaternary record in the Atlantic sector of the southern oceans, Proc. Ocean Drilling Program, Scientific Results, 114, 551–576.

Opoku-Ankomah, Y., Cordery, I., 1993. Temporal variation between New South Wales rainfall and the Southern Oscillation, Int. J. Climatol., 13, 51–64.

Ott, E., 1981. Strange attractors and chaotic motions of dynamical systems, Rev. Mod. Phys., 53 (4/1), 655–671.

Piechota, T.C., Dracup, J.A., 1996. Drought and regional hydrologic variation in the United States: associations with the El Ni ño–Southern Oscillation, Water Resour. Res., 32 (5), 1359–1373.

Rodriguez-Iturbe, I., de Power, B.F., Sharifi, M.B., Georgakakos, K.P., 1989. Chaos in rainfall, Water Resour. Res., 25 (7), 1667–1675.

Ropelewski, C.F., Jones, P.D., 1987. An extension of the Tahiti–Darwin Southern Oscillation index, Mon. Wea. Rev., 115, 2161–2165.

Scargle, J.D., 1990. Studies in astronomical time series analysis, IV: modeling chaotic and random processes with linear filters, Astrophys. J., 359, 469–482.

Schreiber, T., 1993. Extremely simple nonlinear noise-reduction method, Phys. Rev. E, 47 (4), 2401–2404.

Stone, R., Hammer, G.L., Marcussen, T., 1996. Prediction of global rainfall probabilities using phases of the Southern Oscillation Index, Nature, 384 (21), 252–255.

Sugihara, G., May, R.M., 1990. Nonlinear forecasting as a way of distinguishing chaos from measurement error in time series, Nature, 344 (19), 734–741.

Trenberth, K.E., 1984. Signal versus noise in the Southern Oscillation, Mon. Wea. Rev., 112, 326–332.

Troup, A.J., 1965. The ''southern oscillation'', Quart. J. Roy. Meteor. Soc., 91 (390), 490–506.

Tsonis, A.A., Elsner, J.B., Georgakakos, K.P., 1993. Estimating the dimension of weather and climate attractors: important issues about the procedure and interpretation, J. Atmos. Sci., 50 (15), 2549–2555.

Tziperman, E., Stone, L., Cane, M.A., Jarosh, H., 1994. El Niño chaos: overlapping of resonances between the seasonal cycle and the Pacific ocean–atmosphere oscillator, Science, 264, 72–74.

Wolf, A., Swift, J.B., Swinney, H.L., Vastano, J.A., 1985. Determining Lyapunov exponents from a time series, Physica, 16D, 285–317.

Zebiak, S.E., Cane, M.A., 1987. A model El Niño–Southern Oscillation, Mon. Wea. Rev., 115, 2262–2278.